Long-term persistence and multifractality of precipitation and river runoff records

Jan W. Kantelhardt,[1] Eva Koscielny-Bunde, Diego Rybski, Peter Braun,[2] Armin Bunde, and Shlomo Havlin[3]

Institut für Theoretische Physik III, Justus-Liebig-Universität, Giessen, Germany

[1] We discuss and compare the multifractal temporal scaling properties of precipitation and river discharge records on large timescales. To detect long-term correlations and multifractal behavior in the presence of trends, we apply recently developed methods (detrended fluctuation analysis (DFA) and multifractal DFA) that can systematically detect nonstationarities and overcome trends in the data at all timescales. We find that above some crossover time that usually is several weeks, the daily runoffs are characterized by an asymptotic scaling exponent that indicates a slow power law decay of the runoff autocorrelation function and varies from river to river in a wide range. Below the crossovers, pronounced short-term correlations occur. In contrast, most of the precipitation series show scaling behavior corresponding to a rapid decay of the autocorrelation function. For the multifractal characterization of the data we determine the generalized Hurst exponents and fit them by three operational models. While the fits based on the universal multifractal model describe well the scaling behavior of the positive moments in nearly all runoff and precipitation records, positive as well as negative moments are consistent with two-parameter fits from a modified version of the multiplicative cascade model for all runoff records and most of the precipitation records. For some precipitation records with weak multifractality, however, a simple bifractal characterization gives the best fit of the data.

1. Introduction

[2] The persistence analysis of river flows and precipitation has been initiated, about half a century ago, by H. E. Hurst, who found that runoff records from various rivers exhibit "long-range statistical dependencies" [*Hurst*, 1951]. Later, similar long-term correlated fluctuation behavior has also been reported for many other geophysical records including temperature and precipitation data [*Hurst et al.*, 1965; *Mandelbrot and Wallis*, 1969; *Lovejoy and Mandelbrot*, 1985; *Koscielny-Bunde et al.*, 1998; *Matsoukas et al.*, 2000; see also *Feder*, 1988]. The earlier approaches exclusively focused on either the absolute values or the variances of the full distribution of the fluctuations, which can be regarded as the first moment $F_1(s)$ and the second moment $F_2(s)$ of the fluctuations, respectively, in given time segments of length s. In the last years, however, Hurst's original Rescaled Range (R/S) Analysis as well as the spectral analysis have been criticized since both may lead to spurious results in the presence of trends. For a critical discussion of the "Hurst phenomenon" and alternative explanations we refer to *Feller* [1951], *Klemes* [1974], *Potter* [1976], *Salas et al.* [1979], *Bhatthacharya et al.* [1983], *Künsch* [1986], *Bhatthacharya and Waymire* [1990], *Mesa and Poveda* [1993], and references therein.

[3] In the last decade it has been realized that a multifractal description is required for both precipitation and runoff records [*Tessier et al.*, 1993; *Lovejoy and Schertzer*, 1995; *Tessier et al.*, 1996; *Pandey et al.*, 1998; *Douglas and Barros*, 2003], and all moments $F_q(s)$ need to be studied for a full characterization of the fluctuations in these records. For each precipitation or runoff record, this multifractal description can be regarded as a "fingerprint," which, among other things, can serve as an efficient nontrivial test bed for the performance of state-of-the-art precipitation-runoff models. Here, we apply the recently developed Detrended Fluctuation Analysis (DFA) [*Peng et al.*, 1994; *Bunde et al.*, 2000; *Kantelhardt et al.*, 2001] and its multifractal generalization [*Kantelhardt et al.*, 2002] that can systematically distinguish between long-term correlations and trends. This way, we can study the correlation behavior and determine the multifractal spectrum in the presence of

---

trends and compare the long-term scaling behavior of both, daily precipitation and daily runoff records on the same timescales. Our study has also been motivated by the fact that the results for precipitation data have been discussed controversially in literature. On the basis of power spectra analysis, *Fraedrich and Larner* [1993] observed white noise behavior at intermediate scales and long-term correlations ("pink noise") on timescales above three years. *Lovejoy and Mandelbrot* [1985], *Matsoukas et al.* [2000], *Peters et al.* [2002], and *Peters and Christensen* [2002] reported fractal scaling and long-term correlations on timescales below three years. For more recent works on the crossovers in the scaling behavior of rainfall we refer to *Marani* [2003] and *Douglas and Barros* [2003].

[4] Using the detrending methods, we have studied 99 long daily precipitation records and 42 long daily runoff records from all over the world. We find that $F_2(s)$ scales as $s^{h(2)}$ for large time lags s. For the precipitation data, $h(2)$ is close to 0.5, indicating rapidly decaying autocorrelations. We like to note, however, that this result is not synonymous with white noise behavior, since the precipitation data exhibit weak short-term correlations and pronounced multifractal behavior (see below). For the runoff data, in contrast, the fluctuations show a pronounced crossover at intermediate scales (typically several weeks, see *Koscielny-Bunde et al.* [2006]). Below the crossover, for small time windows s, $h(2)$ is close to 1.5, characterizing a highly correlated regime similar to Brownian noise in agreement with the findings of *Matsoukas et al.* [2000]. Well above the crossover, at large times, the scaling exponent $h(2)$ varies from river to river between 0.55 and 0.95 in a nonuniversal manner always remaining in the stationary regime ($h(2) < 1$). Our findings are not consistent with the hypothesis that the scaling is universal with an exponent close to 0.75 [*Hurst et al.*, 1965; *Feder*, 1988; *Peters et al.*, 2002; *Peters and Christensen*, 2002] for both, small and large timescales.

[5] For a full characterization of the records, we studied $F_q(s)$ for a wide range of moments q. A detailed description of the method, which is a multifractal generalization of the DFA, is given in section 2. Our approach differs from the multifractal approach introduced into hydrology by D. Schertzer, S. Lovejoy, A. Davis, and coworkers [*Schertzer and Lovejoy*, 1987, 1991; *Lavallee et al.*, 1993; *Tessier et al.*, 1993, 1996; *Davis et al.*, 1994, 1996; *Schertzer et al.*, 1997; *Pandey et al.*, 1998], which was based on the concept of scale invariance in turbulence [*Frisch and Parisi*, 1985], and trace moment techniques; see also *Rodriguez-Iturbe and Rinaldo* [1997]. Here we perform the multifractal analysis by studying how all moments of the fluctuations $F_q(s) \sim s^{h(q)}$ scale with time s in the asymptotic regime [*Kantelhardt et al.*, 2002; *Koscielny-Bunde et al.*, 2006]. Our approach includes also negative q values and is not based on any specific model assumptions. To describe the numerical outcome of the analysis for $h(q)$ of both precipitation and runoff records, we employed three fitting formulas derived from operational models, (1) the universal multifractal model by *Schertzer and Lovejoy* [1991], which is constrained to $q > 0$, (2) a modified multiplicative cascade model [*Koscielny-Bunde et al.*, 2006], and (3) a bifractal model. We find that the

universal multifractal model (three fitting parameters) can be used to describe well the scaling behavior for the positive moments q of runoff and precipitation records. Both, positive and negative moments, however, follow rather closely the formula from the modified multiplicative cascade model, which has just two fitting parameters, for all runoff records and 55% of the analyzed precipitation records. Some of the precipitation records exhibit rather weak multifractality and 27% of them can be better characterized by the bifractal description.

[6] The paper is organized as follows: In section 2 we describe the detrended fluctuation analysis method and its generalization for multifractal analysis, which we compare with related multifractal formalisms in section 3. Then we report and discuss our results for the correlation behavior of the precipitation and runoff data in section 4, while section 5 presents the results of the multifractal analysis. Finally, the main results are summarized in section 6.

2. Data and Methods

[7] We have analyzed long daily precipitation records $\{P_i\}$ from 99 meteorological stations and long daily runoff records $\{W_i\}$ from 42 hydrological stations. The stations are representative for different rivers and different climate zones. The 99 precipitation records we analyzed were measured at sites in Europe (40), Asia (34), North America (15), Australia (5), and South America (5). The latitude of the locations varies between 52.6°S (Campbell Island, New Zealand) and 71.3°N (Barrow Post, United States). The sites are concentrated on the Northern Hemisphere; thus the average latitude is 41°N. Further, the sites are located on altitudes from sea level up to 3650 m (Lhasa, China) with an average of about 400 m. Concerning the climate, 33 sites are located in maritime regions, 56 in continental climate, and 10 in high continental climate. In other categories, the stations are sited in tropical (12), subtropical (24), warm (44), cold (13), and polar (6) climate. In terms of humidity, the climate is really arid at only one considered site (Kizil Arvat, Turkmenistan), but semiarid at 20 sites, semihumid at 59 sites, and humid at 19 sites. The duration of the records ranges from 34 to 189 years (average 86 years), yielding between ≈12,000 and 69,000 data points each.

[8] Of the 42 daily runoff records, 18 are from the southern part of Germany, and 24 are from North and South America, Africa, Australia, Asia and Europe [see also *Koscielny-Bunde et al.*, 2006]. The duration of the records ranges from 39 to 111 years (average 77 years) for the records from the southern part of Germany and from 51 to 171 years (average 92 years) for the international records, yielding between ≈14,000 and 62,000 data points each. The basin area sizes vary between 390 km² and 3,475,000 km²; the averages are 7400 km² and 350,000 km² for the rivers in southern Germany and the international rivers, respectively.

[9] To eliminate the periodic seasonal trend, we concentrated on the departures

$$\phi_i^{(P)} = P_i - \overline{P}_i \quad \text{and} \quad \phi_i^{(W)} = W_i - \overline{W}_i \tag{1}$$

from the mean daily precipitation $\overline{P}_i$ or runoff $\overline{W}_i$. $\overline{P}_i$ and $\overline{W}_i$ are calculated for each calendar date i, e.g., 1st of April, by
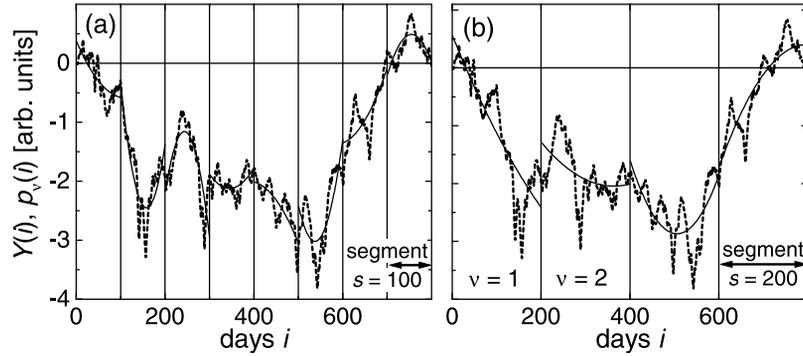
Figure 1. Illustration of the detrending procedure in the second-order detrended fluctuation analysis (DFA2). The profile $Y(i)$ (dashed lines) calculated by summation of the time series is split into nonoverlapping segments of equal duration (timescale) s. This step is illustrated (a) for $s = 100$ days and (b) for $s = 200$ days. Least squares quadratic fits (continuous lines) to the profile are calculated in each segment. The squares of the differences between the profile and the fits are used to calculate the fluctuation function $F(s)$ of the DFA procedure.

averaging over all years in the record. To eliminate the remaining seasonal trend in $(\phi_i^{(P)})^2$ (and $(\phi_i^{(W)})^2$), one may consider dividing $P_i - \overline{P}_i$ (and $W_i - \overline{W}_i$) by the standard deviation for each calendar date, i.e.,

$$\phi_i^{(P)} = \frac{P_i - \overline{P}_i}{\left(\overline{P_i^2} - \overline{P}_i^2\right)^{1/2}} \quad \text{and} \quad \phi_i^{(W)} = \frac{W_i - \overline{W}_i}{\left(\overline{W_i^2} - \overline{W}_i^2\right)^{1/2}}. \quad (2)$$

In order to avoid repetitions we will skip the indices (P) and (W) in all equations that apply to both $\phi_i^{(P)}$ and $\phi_i^{(W)}$ from now on. Quantitatively, correlations within the precipitation or runoff departures separated by s days are defined by the (auto)correlation function,

$$C(s) \equiv \frac{\langle \phi_i \phi_{i+s} \rangle}{\langle \phi^2 \rangle} = \frac{1}{(N-s)\langle \phi^2 \rangle} \sum_{i=1}^{N-s} \phi_i \phi_{i+s}, \quad (3)$$

where N is the number of days in the considered record. We call the ϕ_i uncorrelated, if $C(s)$ is zero for s positive. If correlations exist up to a certain number $s_\times$ of days, the correlation function will be positive up to $s_\times$ and vanish above $s_\times$. For the relevant case of long-term correlations, $C(s)$ decays as a power law,

$$C(s) \sim s^{-\gamma}, \quad 0 < \gamma \leq 1, \quad (4)$$

such that the mean correlation time $\bar{s} = \int_0^\infty ds\, C(s)$ diverges. For $\gamma > 1$, the data are only short-term correlated, since $\bar{s}$ remains finite. For large lag times s, a direct calculation of $C(s)$ is hindered by possible trends in the data. In addition, $C(s)$ becomes unstable because of the finite length of the records. Furthermore, it is difficult to distinguish trends from long-term correlations, because stationary long-term correlated time series exhibit persistent behavior and a tendency to stay close to the momentary value. This causes positive or negative deviations from the average

value for long periods that might look like a trend. For a discussion of these problems, see also the early work of *Klemes* [1974].

[10] To overcome these problems, we have applied the DFA method [*Peng et al.*, 1994; *Bunde et al.*, 2000]. In recent years this method has become a widely used technique for the detection of long-term correlations in noisy, nonstationary time series [*Kantelhardt et al.*, 2001; *Hu et al.*, 2001; *Chen et al.*, 2002]. It has successfully been applied to diverse fields such as DNA sequences [*Peng et al.*, 1994], heart rate dynamics, neuron spiking, human gait, long weather records [*Koscielny-Bunde et al.*, 1998; *Talkner and Weber*, 2000], cloud structure, geology, ethnology, economics time series, and solid state physics (for further references, see, e.g., *Bunde et al.* [2002]).

[11] The DFA procedure consists of four steps. First we determine the "profile"

$$Y(i) \equiv \sum_{k=1}^{i} \phi_k, \quad i = 1, \ldots, N, \quad (5)$$

of the data series ϕ_k of length N. The cumulative sum generates a nonstationary profile $Y(i)$. In the DFA method (as well as in Hurst's original Rescaled Range Analysis), data has to be turned nonstationary, since the scaling is determined from a mean-square displacement type quantity. In contrast, some of the methods used in geophysics and turbulence [*Schertzer and Lovejoy*, 1987, 1991; *Lavallee et al.*, 1993; *Tessier et al.*, 1993, 1996; *Davis et al.*, 1994, 1996; *Schertzer et al.*, 1997; *Pandey et al.*, 1998] require stationary series, which are often generated by differentiation.

[12] Second we divide the profile $Y(i)$ into $N_s \equiv \text{int}(N/s)$ nonoverlapping segments of equal length s. This is illustrated for two scales s in Figure 1. Since the length N of the series is usually not a multiple of the considered timescale s, a short part at the end of the profile may remain. In order not to disregard this part of the series, the same procedure is repeated starting from the opposite end. Thereby, $2N_s$ segments are obtained altogether.

[13] In the third step we calculate the local trend for each of the $2N_s$ segments by fitting (least squares fit) a polynomial of order n to the data and determine the variance

$$\sigma(\nu, s) \equiv \frac{1}{s} \sum_{i=1}^{s} [Y((\nu - 1)s + i) - p_\nu(i)]^2 \qquad (6)$$

for each segment ν, $\nu = 1, \ldots, 2N_s$. Here, $p_\nu(i)$ is the fitting polynomial representing the local trend in the segment ν. Linear, quadratic, cubic, or higher-order polynomials can be used in the fitting procedure. When linear polynomials are used, the fluctuation analysis is called DFA1, for quadratic polynomials we have DFA2, for cubic polynomials DFA3, etc.; see *Bunde et al.* [2000]. The quadratic fitting procedure used in DFA2 is illustrated in Figure 1. DFA2 removes quadratic trends in the profile $Y(i)$ and thus linear trends in the original series ϕ_i.

[14] In the fourth step we average the variances of all segments and take the square root to obtain the mean fluctuation function,

$$F(s) \equiv \left[\frac{1}{2N_s} \sum_{\nu=1}^{2N_s} \sigma(\nu, s) \right]^{1/2}. \qquad (7)$$

We are interested in how $F(s)$ depends on the timescale s. Hence we have to repeat steps 2 to 4 for several timescales s. It is apparent that $F(s)$ will increase with increasing s. If the ϕ_i are long-term power law correlated according to equation (4), $F(s)$ increases, for large values of s, by a power law [*Feder*, 1988; *Peng et al.*, 1994; *Kantelhardt et al.*, 2001],

$$F(s) \sim s^{h(2)} \qquad (8)$$

with

$$h(2) = \begin{cases} 1 - \gamma/2, & \text{for } 0 < \gamma < 1, \\ 1/2, & \text{for } \gamma \geq 1. \end{cases} \qquad (9)$$

Accordingly, when the autocorrelation function decreases faster than $1/s$ in time, we asymptotically have $F(s) \sim s^{1/2}$. For short-term correlated data described, e.g., by equation (4) with $\gamma > 1$ or by an exponential decay, a crossover to $h(2) = 1/2$ occurs above the correlation time $\bar{s}$. If the time series ϕ_i is stationary, we can also apply standard spectral analysis techniques and calculate the power spectrum $S(f)$ as a function of the frequency f. The exponent β in the scaling law $S(f) \sim f^{-\beta}$ is related to the mean fluctuation function exponent $h(2)$ by $\beta = 2h(2) - 1$ [*Rangarajan and Ding*, 2000; *Kantelhardt et al.*, 2001].

[15] For multifractal time series, a single scaling exponent like $h(2)$ or γ does not completely characterize the record, since many subsets of the series have different scaling behavior, e.g., large fluctuations are less correlated than small fluctuations. In order to study these multifractal scaling properties, the DFA procedure can be generalized to higher moments [*Kantelhardt et al.*, 2002]. This generalization (multifractal DFA, MF-DFA) is equivalent to the wavelet transform modulus maxima (WTMM) method [*Muzy et al.*, 1991; *Arneodo et al.*, 2002], but the

MF-DFA is much easier to implement on the computer; see *Kantelhardt et al.* [2003] for a comparison of the two methods (for wavelet methods, see also *Kumar and Foufoula-Georgiou* [1997]). In this procedure, the variance $\sigma(\nu, s)$ in equation (7) is replaced by its $q/2$-th power and the square root is replaced by the $1/q$-th power, where $q \neq 0$ is a real parameter,

$$F_q(s) \equiv \left[\frac{1}{2N_s} \sum_{\nu=1}^{2N_s} \sigma^{q/2}(\nu, s) \right]^{1/q}. \qquad (10)$$

Analogous to equation (8) one defines then the generalized fluctuation exponent $h(q)$ by

$$F_q(s) \sim s^{h(q)}. \qquad (11)$$

We note that $h(1)$ corresponds to the classical Hurst exponent H determined by Rescaled Range Analysis (since first moments are considered in both cases) and that multifractal DFA is identical to standard DFA if $q = 2$ (hence the notation $h(2)$ in equation (8)).

[16] For monofractal time series, $h(q)$ is independent of q, since the scaling behavior of the variances $\sigma(\nu, s)$ is identical for all segments ν. If, on the other hand, small and large fluctuations scale differently, there will be a significant dependence of $h(q)$ on q: If we consider positive values of q, the segments ν with large variance $\sigma(\nu, s)$ (i.e., large deviations from the corresponding fit) will dominate the average $F_q(s)$. Thus, for positive values of q, $h(q)$ describes the scaling behavior of the segments with large fluctuations. Usually large fluctuations are characterized by a smaller scaling exponent $h(q)$. On the contrary, for negative values of q, the segments ν with small variance $\sigma(\nu, s)$ will dominate the average $F_q(s)$. Hence, for negative values of q, $h(q)$ describes the scaling behavior of the segments with small fluctuations, which are usually characterized by a larger scaling exponent. The multifractal fluctuation exponents $h(q)$ defined in equation (10) are directly related to the classical Renyi exponents $\tau(q)$ [see, e.g., *Feder*, 1988; *Rodriguez-Iturbe and Rinaldo*, 1997] via [*Kantelhardt et al.*, 2002]

$$h(q) = [\tau(q) + 1]/q. \qquad (12)$$

3. Comparison With Related Multifractal Formalisms

[17] In the geophysics literature also other multifractal quantities have been used that $h(q)$ can easily be related to:

[18] (1) The "generalized variogram" $C_q(s)$ (see, e.g., equations (3.82)–(3.84) of *Rodriguez-Iturbe and Rinaldo* [1997] and references therein) is defined as

$$C_q(s) \equiv \langle |Y(i + s) - Y(i)|^q \rangle \sim s^{K(q)}, \qquad (13)$$

where the average is taken over all values of i. Comparing equations (10) and (13) one can easily verify that $h(q)$ and $K(q)$ are related by
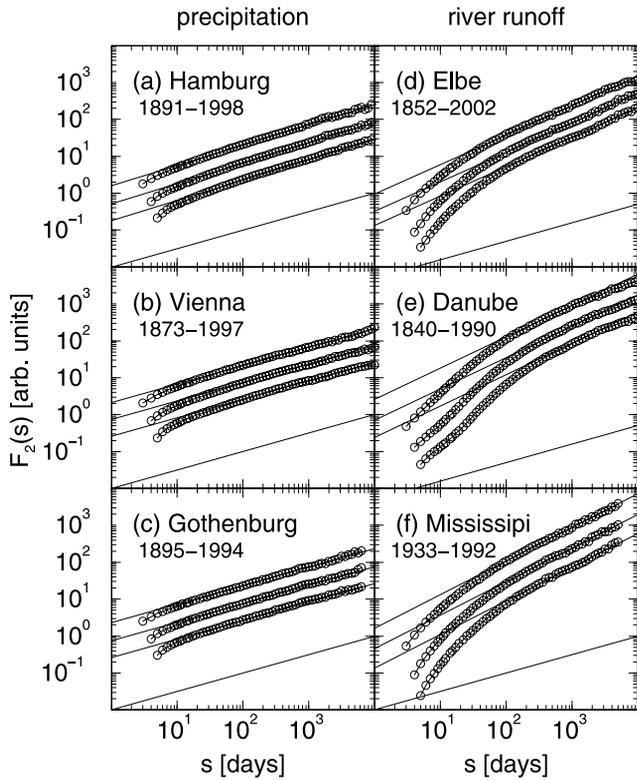
$$K(q) = q h(q). \qquad (14)$$

precipitation   river runoff

Figure 2. Fluctuation functions $F_2(s)$ versus timescale s obtained from DFA1−DFA3 (from top to bottom) in double logarithmic plots for representative precipitation and runoff records (shifted vertically for clarity). Figures 2a−2c show precipitation records: (a) Hamburg, Germany ($h(2) = 0.55 \pm 0.03$), (b) Vienna, Austria ($h(2) = 0.50 \pm 0.03$), and (c) Gothenburg, United States ($h(2) = 0.50 \pm 0.03$). Figures 2d−2f show runoff records: (d) Elbe river in Dresden, Germany ($h(2) = 0.80 \pm 0.03$), (e) Danube river in Orsova, Romania ($h(2) = 0.85 \pm 0.03$), and (f) Mississippi river in St. Louis, United States ($h(2) = 0.91 \pm 0.03$). The straight lines through the data have the reported slopes, and lines with slope $h(2) = 0.5$ are shown below the data for comparison with the uncorrelated case.

[19]   (2) In several geophysics and turbulence papers [see, e.g., *Schertzer and Lovejoy*, 1987, 1991; *Lavallee et al.*, 1993; *Tessier et al.*, 1993, 1996; *Davis et al.*, 1994, 1996; *Schertzer et al.*, 1997; *Pandey et al.*, 1998], the structure function

$$S_q(s) \equiv \langle |\phi_{i+s} - \phi_i|^q \rangle \sim s^{\zeta(q)} = s^{qH(q)} \qquad (15)$$

has been analyzed directly without employing the profile $Y(i)$ as done in equation (13). It is easy to see that $H(q)$ is related to $h(q)$ by

$$H(q) = \zeta(q)/q = h(q) - 1. \qquad (16)$$

Accordingly, the multifractal exponent $H(q)$ defined by *Davis et al.* [1994] and the exponent $h(q)$ defined here in equation (11) differ only by 1. This difference is due to the fact that here we analyze the cumulative sum of ϕ_i, while

Davis et al. as well as the Lovejoy-Schertzer group analyze the ϕ_i directly. For modeling the multifractal behavior, one can employ, for example, a particular multifractal process where $H(q)$ (or $h(q) = H(q) + 1$) is known and adjust the parameters. However, in most multifractal processes $H(1) = 0$ is fixed. Hence one has to use a fractional integration and shift the whole function $H(q)$ to adjust the value for $q = 1$. When doing this, S. Lovejoy and D. Schertzer obtained an interesting formula for $\zeta(q) = qH(q)$ for positive q values (D. Schertzer, private communication, 2004),

$$\zeta(q) = qH' - \frac{C_1}{\alpha' - 1}\left(q^{\alpha'} - q\right), \qquad q \geq 0. \qquad (17)$$

[20]   The great advantage of the MF-DFA method used here is that it includes also negative q values, such that the basic Renyi exponents $\tau(q)$ can be calculated for both negative and positive q values. This allows a further characterization of the multifractal series by the singularity spectrum $f(\alpha)$, which is related to $\tau(q)$ via a Legendre transform [see, e.g., *Feder*, 1988; *Rodriguez-Iturbe and Rinaldo*, 1997],

$$\alpha = \frac{d\tau(q)}{dq} \quad \text{and} \quad f(\alpha) = q\alpha - \tau(q). \qquad (18)$$

Here, α is the singularity strength or Hölder exponent, while $f(\alpha)$ denotes the dimension of the subset of the series that is characterized by α. Using equation (12), we can directly relate α and $f(\alpha)$ to $h(q)$,

$$\alpha = h(q) + q\frac{dh(q)}{dq} \quad \text{and} \quad f(\alpha) = q[\alpha - h(q)] + 1. \qquad (19)$$

The strength of the multifractality of a time series can be characterized by the difference between the maximum and minimum singularity strength α, $\Delta\alpha = \alpha_{max} - \alpha_{min}$, which fulfill $f(\alpha) \rightarrow 0$ for $\alpha \rightarrow \alpha_{max}$ and $\alpha \rightarrow \alpha_{min}$.

4.   Results for the Correlation Behavior

[21]   Figure 2 shows the fluctuation functions $F_2(s)$ obtained from DFA1, DFA2, and DFA3 for three representative daily precipitation records (Figures 2a−2c) and three representative runoff records (Figures 2d−2f). In the log-log plot, the curves are approximately straight lines on large scales s. The runoff fluctuations show a pronounced crossover at timescales of several weeks. We note that the crossover timescale is similar to the period of planetary waves, which are oscillations of very predominantly tropospheric origin with typical periods of about 2−30 days [see, e.g., *Lastovicka et al.*, 2003]. Above the crossover, the fluctuation functions (from DFA1-DFA3) show power law behavior with exponents $h(2) \simeq 0.80$ for the Elbe, $h(2) \simeq 0.85$ for the Danube, and $h(2) \simeq 0.91$ for the Mississippi. Below the crossover, we find an effective scaling exponent $h(2) \approx 1.5$, indicating strong short-term correlations on small timescales. Approximately, the short-term correlations can be modeled by an ARMA process, where the correlation time is represented by the typical decay time of floods. This yields $h(2) = 1.5$ on short timescales in agreement with
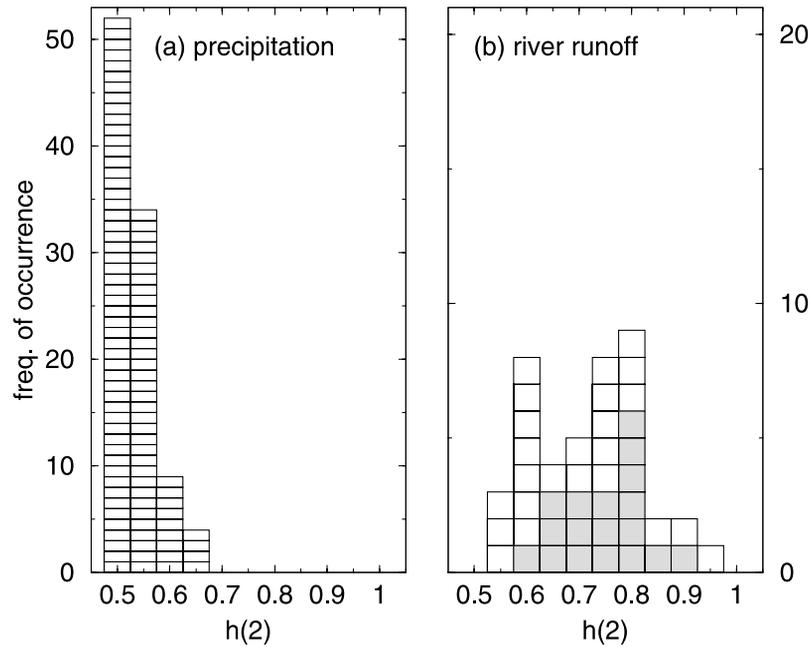
Figure 3. Histograms of the long-term fluctuation exponents $h(2)$ for (a) all 99 daily precipitation records and (b) all 42 daily runoff records, 18 from southern Germany (grey boxes) and 24 from international hydrological stations (white boxes). The scaling exponents have been determined from power law fits of the DFA2 fluctuation function on large timescales. Each box represents the result for one hydrological or meteorological station.

our observation. Note, however, that long-term correlations (and multifractality on large timescales) require an additional and different modeling approach. For the precipitation records there is only a very weak crossover in $F_2(s)$ and the $h(2)$ values are rather close to 0.5, indicating rapidly decaying autocorrelations. Specifically, we find $h(2) \simeq 0.55$ for Hamburg, $h(2) \simeq 0.50$ for Vienna, and $h(2) \simeq 0.50$ for Gothenburg, corresponding to a correlation exponent $\gamma \approx 0.9$ for Hamburg, and $\gamma \geq 1$ for Vienna and Gothenburg. For the precipitation data, the higher slope at very small scales is partly a methodical artifact [Kantelhardt et al., 2001].

[22] Figure 3 shows the distributions of $h(2)$ obtained with DFA2 on large timescales for all 99 precipitation records and all 42 runoff records using equation (1) for seasonal detrending. One can clearly see that most precipitation records exhibit no long-term correlations ($h(2) \approx 0.5$) or only very weak long-term correlations ($h(2) \approx 0.55$); the mean value is $h(2) = 0.53 \pm 0.04$ (see Table 1). We find no systematic dependence of the $h(2)$ values on climate zone or geographical region. In order to confirm the absence of long-term autocorrelations in the precipitation series, we have also calculated the autocorrelation function $C(s)$ (see equation (3)). The representative results in Figure 4 show that all correlations decay after a very small number of days. Note, however, that this result is obtained for the second moment, and thus it refers only to two-point correlations; higher-order correlations are not excluded by our result.

[23] Our results for $h(2)$ are not in agreement with Matsoukas et al. [2000], where, using DFA1 and seasonal detrending based on procedures similar to equation (1) for nine precipitation records with 15 min resolution, $h(2) \approx 1.0$ ($\alpha = h(2)$ in the notation used there) was found on time-

scales below 10 days and $h(2) = 0.6 \ldots 0.8$ on timescales from 10 days to 16 months. We cannot exactly pinpoint the reason for the disagreement, in particular since the binned spectral analysis by Matsoukas et al. [2000] agrees with our results. However, the DFA1 discrepancy might be caused by

Table 1. Details of the Records Analyzed in Figure 5, Figure 6 (Precipitation), and Figure 7 (Runoff) and Average Values for All Records We Studied[a]

	Period	$h(2)$	$\Delta\alpha$	a	b	H'	C_1	α'
Precipitation
Spokane	1881–1994	0.51	0.30	0.63	0.77	−0.48	0.008	1.9
Edinburgh	1896–1997	0.52	0.34	0.61	0.77	−0.47	0.012	1.8
Winnemucca	1877–1994	0.50	0.33	0.63	0.79	−0.49	0.009	2.2
Jena	1827–2000	0.56	0.11	–	–	−0.43	0.006	2.3
Average (99 records)	86 years	0.53	0.29	–	–	−0.45	0.012	2.0
Standard deviation	33 years	0.04	0.14	–	–	0.06	0.010	0.4
Runoff
Weser	1823–1993	0.76	0.43	0.50	0.68	−0.24	0.023	1.7
Fraser	1913–1996	0.69	0.38	0.53	0.70	−0.29	0.017	1.7
Susquehanna	1891–1986	0.58	0.48	0.55	0.77	−0.40	0.018	1.7
Niger	1907–1985	0.60	0.62	0.51	0.78	−0.35	0.040	1.5
Average (42 records)	86 years	0.72	0.49	–	–	−0.25	0.039	1.4
Standard deviation	27 years	0.11	0.16	–	–	0.10	0.028	0.5

[a]The recording period and the fitting parameters obtained within the modified multiplicative cascade model, equation (21), and the Lovejoy-Schertzer model, equation (20), are reported. Further, our two main parameters, the fluctuation exponents $h(2) = 1 - \gamma/2 = (\beta + 1)/2$ and the resulting multifractality strength $\Delta\alpha$, are given. In the case of Jena, equation (24) has been used instead of equation (21), and the corresponding parameters are $\alpha_1 = 0.57$, $\alpha_2 = 0.45$, and $q_\times = 3.3$.
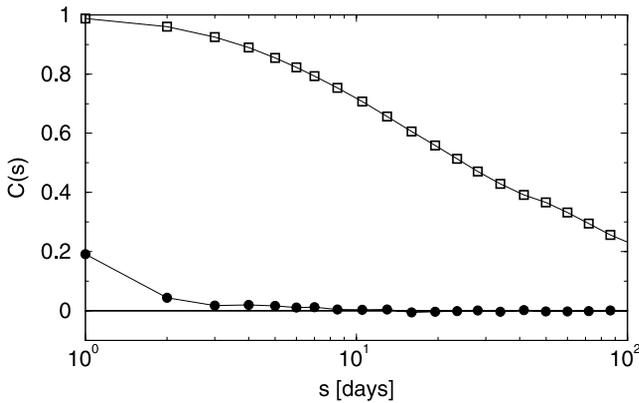
Figure 4. Autocorrelation function $C(s)$ for one representative precipitation record (Vienna, circles) and one representative runoff record (Mississippi, squares). The autocorrelations of the precipitation data disappear after a few days.

the shorter time series considered by *Matsoukas et al.* [2000]. Our $h(2)$ values are also not in agreement with *Peters et al.* [2002] and *Peters and Christensen* [2002], where records of length six months were considered and an exponent $h(1) \approx 0.76$ ($H = h(1) \gtrsim h(2)$) was found using Rescaled Range Analysis. We believe that the reason for this disagreement is that the seasonal trend cannot be eliminated in these short records and acts like a long-term correlation. Thus it seems that the larger exponent obtained by Peters et al. is due to the seasonal trend but not to long-term correlations. For intermediate timescales up to three years, our finding is in agreement with *Fraedrich and Larner* [1993], who, however, report long-term correlations on even larger timescales in disagreement with our conclusion. This observation of correlations on large timescales might also have been caused by nonstationarities in the data. Finally, we like to note that our results do not change significantly, when also the seasonal trend in the variance of the data was eliminated by using equation (2) instead of equation (1). Although $h(2)$ changes by about ±0.03 for individual records, the average $h(2)$ remains constant.

[24] In remarkable contrast to the precipitation records, most of the runoff records are strongly long-term correlated; the mean value is $h(2) = 0.72$. The individual $h(2)$ values have a very broad distribution (see Figure 3b), which is not significantly more narrow even for the data from a rather small region (southern Germany) with much smaller average basin area. The long-term exponents vary strongly from river to river in an apparently nonsystematic fashion. Accordingly, there is no universal scaling behavior of the runoff data and there is no systematic dependence of the exponents on the size of the basin area. The pronounced variations probably reflect the fact that there exist different mechanisms for floods, and each one may induce different scaling. For example, rain-induced floods and snow-induced floods may introduce different spatial scaling behavior [*Gupta and Dawdy*, 1995], which might also result in different temporal scaling behavior. Our results (based on 3 rivers only) suggest that the contribution of snow melting leads to less correlated runoffs than the contribution of rainfall [*Koscielny-Bunde et al.*, 2006], but more compre-

hensive studies will be needed to confirm this interesting result.

[25] Since the autocorrelations of rainfall data decay rapidly in time, their temporal correlations can neither account for the long-term correlations nor for the broad distribution of the correlation exponents of the runoff data. Our study seems to indicate that the persistence of the runoffs is rather caused by storage effects than by long-term memory of the precipitation; the integration of rainfall in time-space might produce long-term memory in river flows. If this interpretation is correct, i.e., that runoff persistence is caused by catchment storage, we would expect it to be less emphasized in arid regions. Indeed, for the Mary river in Australia, the only river with arid catchment in our study, we find a quite low fluctuation exponent, $h(2) \approx 0.6$, corresponding to weak persistence. However, further studies are needed to confirm our interpretation. It is interesting to compare the nonuniversal long-term correlations of river flow records with climate records, where universal long-term persistence of temperature records at land stations, i.e., rather identical values of $h(2) = 0.66 \pm 0.06$ were observed [*Koscielny-Bunde et al.*, 1998; *Talkner and Weber*, 2000; *Weber and Talkner*, 2001; *Eichner et al.*, 2003].

[26] To confirm that the slope $h(2) > 0.5$ for the runoff data is due to long-term correlations and not due to a broad probability distribution of the values ϕ_i (Joseph phenomenon versus Noah phenomenon, see *Mandelbrot and Wallis* [1968]), we have, in a separate analysis, eliminated the correlations by randomly shuffling the ϕ_i. This shuffling has no effect on the probability distribution function of ϕ_i. We find that the exponent $h(2)$ characterizing the fluctuations in the shuffled records is 1/2, indicating that the Joseph phenomenon is the main effect.

[27] We also checked if the results changed when also the seasonal trend in the variance of the data was eliminated according to equation (2). We obtained an increase of $h(2)$ between 0.1 and 0.25 for those rivers that show a strong seasonal dependence of the runoffs, with pronounced flooding in one season and (nearly) vanishing runoffs in another season. We come back to this point at the end of the subsequent section.

5. Multifractal Characterization

[28] Next we compare the multifractal behavior of the 99 daily precipitation records with those of the 42 daily river runoff records. For all records, we find that MF-DFA2, MF-DFA3, and MF-DFA4 (corresponding to second-, third-, and fourth-order polynomials in the detrending procedure, respectively) yield similar results for the fluctuation function $F_q(s)$. Therefore we present only the results for MF-DFA2. Again we begin with the seasonal detrending according to equation (1). Figure 5 shows two representative examples for the MF-DFA2 fluctuation functions $F_q(s)$, for the precipitation record at Spokane, United States (Figure 5a) and the runoff record of the Weser river (Figure 5b). The standard fluctuation function $F_2(s)$ is plotted with crosses. The crossover in $F_2(s)$ for the runoff data that was discussed in the previous section can also be seen in the other moments, and additionally a similar crossover can be seen in the negative moments for the precipitation data. The position of the crossover increases monotonically with
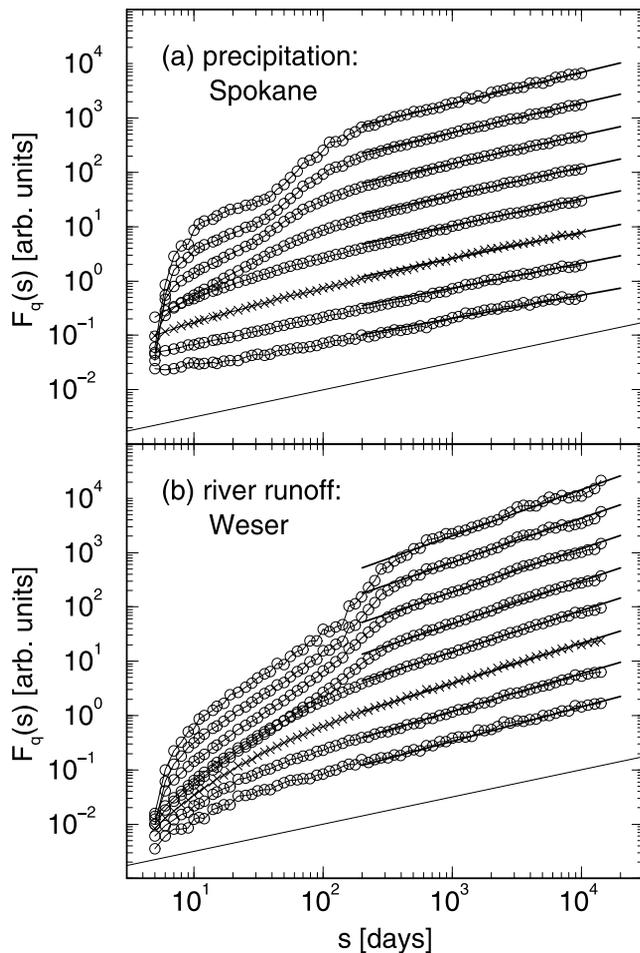
Figure 5. Multifractal fluctuation functions $F_q(s)$ versus timescale s obtained from multifractal DFA2 for two representative records: (a) precipitation at Spokane, United States, and (b) river Weser in Vlotho, Germany. The curves correspond to different values of q, $q = -8, -4, -2, -1, 1, 2, 4, 8$ (from top to bottom) and are shifted vertically for clarity. The curve for $q = 2$ (standard DFA) is plotted with crosses. The straight lines through the data are the linear fits we use to calculate $h(q)$ (as reported in Figures 6 and 7), and additional thin lines with slope $h(2) = 0.5$ are shown below the data for comparison with the uncorrelated case.

decreasing q and the crossover becomes more pronounced. While most of the recent literature focussed on short-term multifractality and the crossovers occurring on timescales below one year [*Lovejoy and Schertzer*, 1995; *Tessier et al.*, 1996; *Harris et al.*, 1996; *Pandey et al.*, 1998; *Olsson et al.*, 1999; *Deidda et al.*, 1999; *Deidda*, 2000; *Douglas and Barros*, 2003], here we are mainly interested in the asymptotic behavior of $F_q(s)$ at large times s. One can see clearly that above the crossover, the $F_q(s)$ functions are straight lines in the double logarithmic plot, and the slopes increase slightly when going from high positive moments toward high negative moments (from the bottom to the top). For the precipitation at Spokane (Figure 5a), for example, the slope changes from 0.42 for $q = 8$ to 0.57 for $q = -8$. The monotonous increase of the slopes, $h(q)$, is the signature of multifractality. We obtain similar increases for the runoff

records, although all $h(q)$ are larger on the average; for the Weser river the results are $h(8) = 0.63$ and $h(-8) = 0.84$ (see Figure 5b).

[29] From the asymptotic slopes of the curves in Figure 5 (see linear fits in the plots), we obtained the generalized Hurst exponents $h(q)$, which are plotted versus the moment q in Figure 6 for four representative precipitation records and in Figure 7 for four representative runoff records; see Table 1 for details.

[30] Our results for $h(q) = [\tau(q) + 1]/q$ may be compared with several functional forms used in the literature to describe multifractality. First we consider the formula (see equations (16) and (17))

$$ h(q) = H' + 1 - \frac{C_1}{\alpha' - 1} \left(q^{\alpha' - 1} - 1 \right), \qquad q \geq 0, \qquad (20) $$

with the three parameters H', C_1, and α', that has been successfully used by S. Lovejoy, D. Schertzer, and coworkers [*Schertzer and Lovejoy*, 1987, 1991; *Lavallee et al.*, 1993; *Tessier et al.*, 1993, 1996; *Schertzer et al.*, 1997; *Pandey et al.*, 1998; see also *Douglas and Barros*, 2003] to describe the multifractal behavior of rainfall and runoff records at smaller timescales. Of course, the functional form (20) does apply only to positive moments q. The lines in the upper right parts of Figures 6 and 7 indicate the corresponding fits, and the values of the three parameters are listed in Table 1 together with their means for all precipitation and runoff records.

[31] Figure 8 summarizes our results for H', C_1, and α', for both precipitation and runoff records. For the precipitation data, we obtained $H' = -0.45 \pm 0.06$, $C_1 = 0.01 \pm 0.01$, and $\alpha' = 2.0 \pm 0.4$, while the runoff data yielded $H' = -0.25 \pm 0.10$, $C_1 = 0.04 \pm 0.03$, and $\alpha' = 1.4 \pm 0.5$.

[32] Our values for H' are in marginal agreement with earlier studies by *Tessier et al.* [1996], who obtained $H' = -0.35 \pm 0.2$ for precipitation records and $H' = -0.05 \pm 0.2$ for runoff records. The same conclusion holds for *Pandey et al.* [1998], who reported $H' = -0.03 \pm 0.14$ for runoff records. The agreement is surprising, since in these earlier studies a seasonal detrending (our equations (1) and (2)) has not been performed. The multifractality is characterized by the parameters C_1 and α'. Here, *Tessier et al.* [1996] report $\alpha' = 1.6 \pm 0.2$ and $C_1 = 0.10 \pm 0.05$ for precipitation and $\alpha' = 1.45 \pm 0.2$ and $C_1 = 0.2 \pm 0.1$ for river flows, while *Pandey et al.* [1998] obtained $\alpha' = 1.7 \pm 0.11$ and $C_1 = 0.12 \pm 0.03$ for river flows. In a more recent study, *Tchiguirinskaia et al.* [2002] analyzed several runoff records in Russia, finding $\alpha' \approx 1.7$ and $C_1 \approx 0.03$. Our results for the exponent α' are, within the error bars, in agreement with these earlier studies. The result for C_1 is in agreement with *Tchiguirinskaia et al.* [2002], but disagrees with *Tessier et al.* [1996] and *Pandey et al.* [1998], who did not explicitly focus on the asymptotic regime and therefore obtained larger parameters C_1 (as given by *Tchiguirinskaia et al.* [2002] for the short-term regime).

[33] *Tessier et al.* [1996] concluded that the H' values for precipitation and for runoff differ by $\Delta H' = \Delta h \approx 0.3$, while the α' and C_1 values are compatible. We find a similar difference in the Hurst exponents, $\Delta h \approx 0.2$. Our α' and C_1 values for precipitation and runoff seem to be marginally compatible, since the corresponding histograms in Figure 8
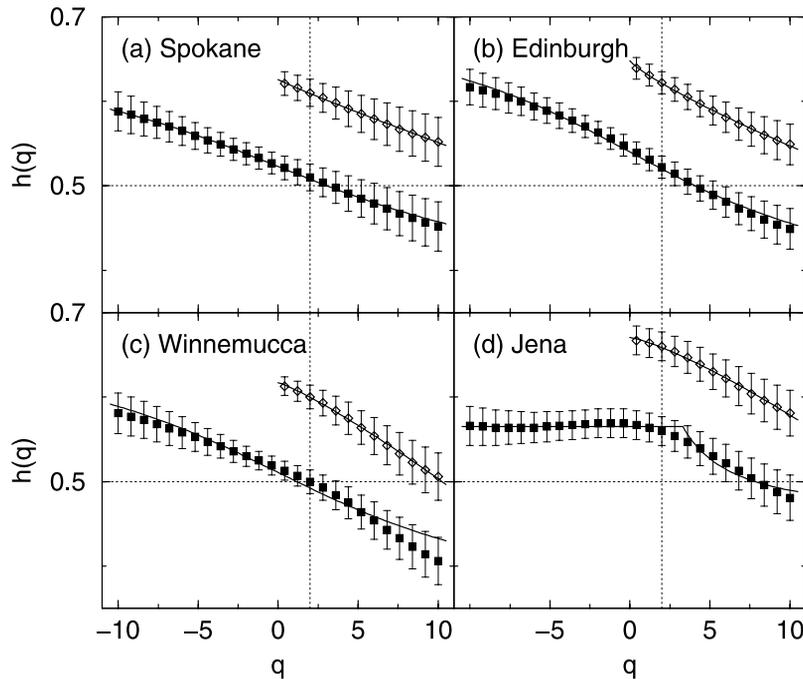
Figure 6. Generalized Hurst exponents $h(q)$ for four representative daily precipitation records: (a) Spokane (United States), (b) Edinburgh (UK), (c) Winnemucca (United States), and (d) Jena (Germany). The $h(q)$ values (solid symbols) have been determined by straight line fits of log-log plots of $F_q(s)$ on large timescales s. The solid lines through the solid symbols are fits to the data using the operational modified multiplicative cascade model, equation (21), except for Figure 6d, where the bifractal model, equation (24), has been used instead. In this case the corresponding parameters are $\alpha_1 = 0.57$, $\alpha_2 = 0.45$, and $q_\times = 3.3$. The record in Figure 6c is an example where the modified multiplicative cascade model fits rather poorly. In the upper right corner of each plot $h(q)$ is shown (open symbols, shifted upward by 0.1) together with fits using the Lovejoy-Schertzer model, equation (20). The straight dotted lines indicate uncorrelated behavior $h = 0.5$ and $q = 2$, respectively.

are shifted to the left and to the right, respectively, for the runoff data. The average of C_1 is more than three times larger for runoff. Thus we conclude that the runoff fluctuations cannot be generated by a simple fractional (time) integration of rainfall series. We believe that storage effects and the highly intermittent spatial behavior of rainfall as well as the highly nonlinear interaction between rainfall and runoff have to be taken into account here.

[34] Next we consider the functional form

$$\tau(q) = -\frac{\ln(a^q + b^q)}{\ln 2} \quad \text{or} \quad h(q) = \frac{1}{q} - \frac{\ln(a^q + b^q)}{q \ln 2}, \quad (21)$$

which can be derived from a modification of the multiplicative cascade model [*Koscielny-Bunde et al.*, 2006]. The advantage of this formula is that it extends also to negative q values, and thus can be used for obtaining the multifractal spectrum $f(\alpha)$. By equation (21), the infinite number of exponents $h(q)$ can be described by only two independent parameters, a and b; the width of the corresponding singularity spectrum (see equation (19)) is given by $\Delta\alpha = |\ln a - \ln b|/\ln 2$. Our fitting results for the examples shown in Figures 6 and 7 are listed in Table 1, except for the Jena record, where equation (21) does not provide a reasonable fit. The two parameters a and b can then be regarded as multifractal fingerprint for a considered runoff or precipita-

tion record. This is particularly important for evaluating precipitation-runoff models, for example artificial rainfall data (input for the models) can be generated with these two parameters and then the runoff (output of the models) can be checked on the basis of them.

[35] It is important to emphasize that the parameters a and b have been obtained from the asymptotic part of the generalized fluctuation function, and are therefore not affected by seasonal dependencies, which cannot be fully eliminated from the data. We would like to note that different multifractal models for high-resolution precipitation time series, which include the crossover on short timescales, have been suggested by *Veneziano et al.* [1996], *Schmitt et al.* [1998], *Deidda et al.* [1999], *Deidda* [2000], and *Veneziano and Iacobellis* [2002]. For a model based on self-organized criticality we refer to *Andrade et al.* [1998].

[36] However, for the precipitation records, there are several cases where equation (21) cannot be used to fit $h(q)$ for all q values. In some of these cases (like the Jena precipitation record), a simple bifractal model fits much better to the $h(q)$ data. For bifractal records the Renyi exponents $\tau(q)$ are characterized by two distinct slopes α_1 and α_2,

$$\tau(q) = \begin{cases} q\alpha_1 - 1 & q \leq q_\times \\ q\alpha_2 + q_\times(\alpha_1 - \alpha_2) - 1 & q > q_\times \end{cases} \quad (22)$$
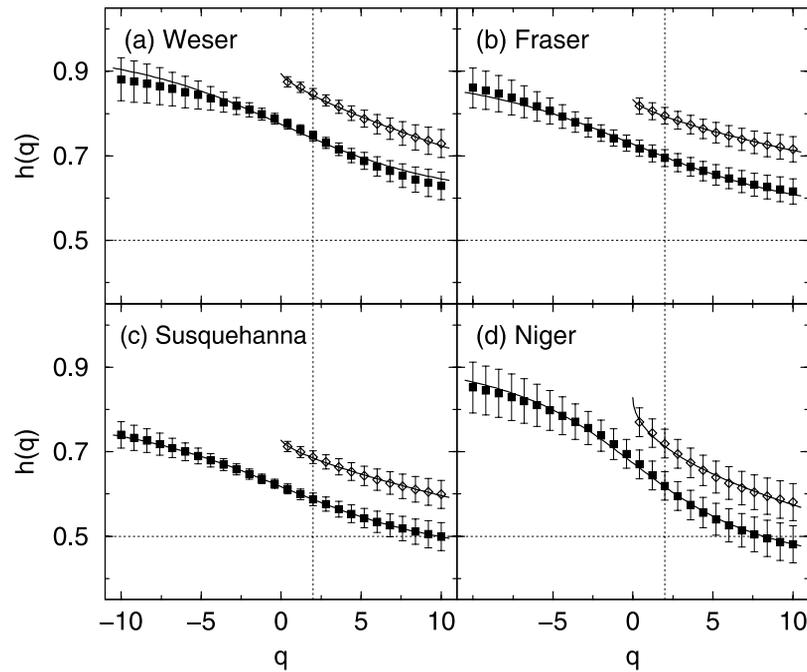
Figure 7. Generalized Hurst exponents $h(q)$ for four representative daily runoff records: (a) Weser in Vlotho, Germany, (b) Fraser in Hope, United States, (c) Susquehanna in Harrisburg, United States, and (d) Niger in Koulikoro, Mali, analogous with Figure 6, except for the range of the $h(q)$ axis. Again, the solid lines are fits to the data using equations (20) and (21), and the straight dotted lines indicate uncorrelated behavior $h = 0.5$ and $q = 2$, respectively.
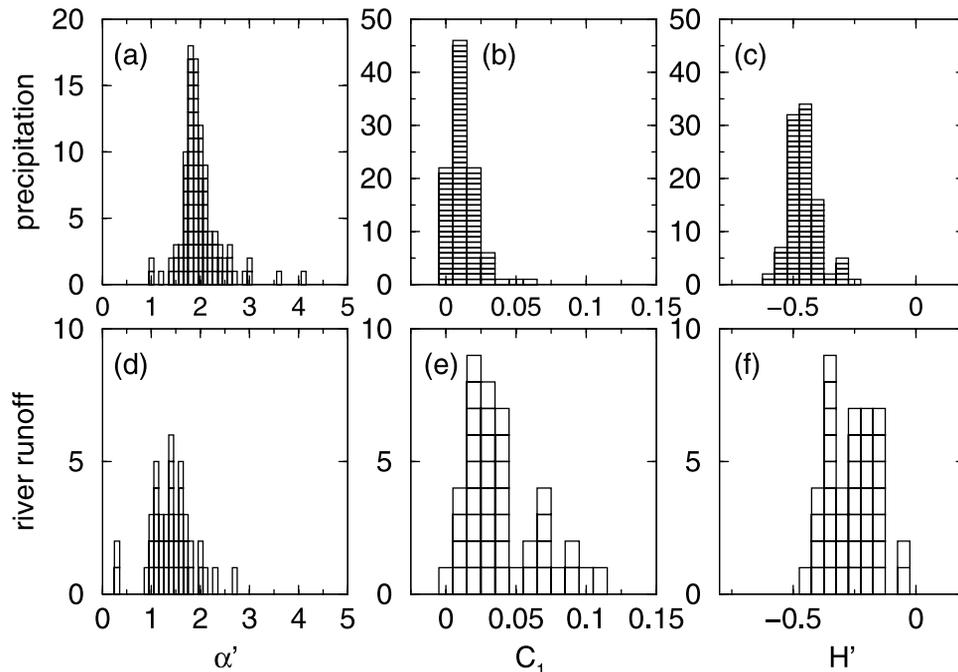

Figure 8. Histograms of the parameters α', C_1, and H' for (a–c) all 99 daily precipitation records and (d–f) all 42 daily runoff records. The values have been determined by applying nonlinear fits of equation (20) to the generalized Hurst exponents $h(q)$. Each box represents the result for one meteorological or hydrological station.
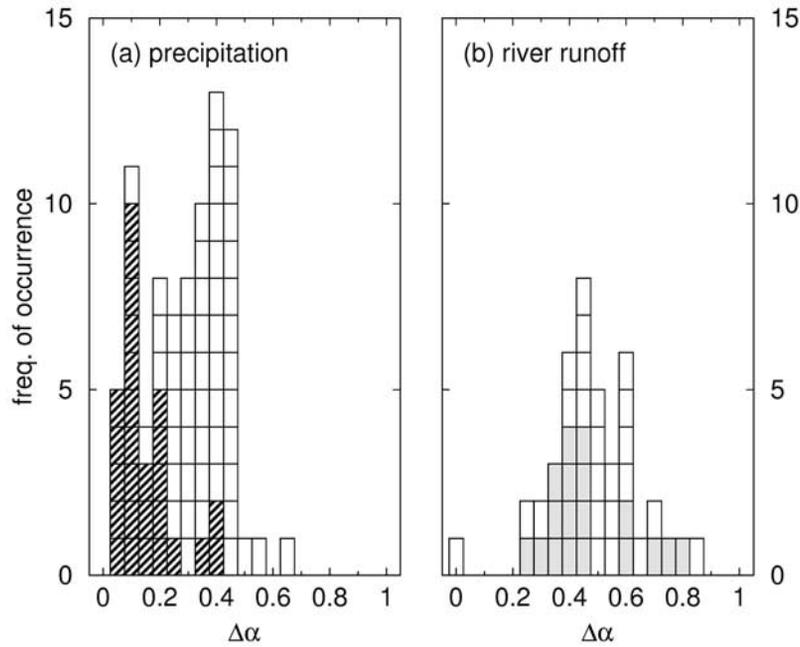
Figure 9. Histograms of the multifractality strength $\Delta\alpha$ for (a) 81 of 99 daily precipitation records and (b) all 42 daily runoff records, 18 from southern Germany (grey boxes) and 24 from international hydrological stations (white boxes). The values have been determined by applying nonlinear fits to the generalized Hurst exponents $h(q)$. Each box represents the result for one meteorological or hydrological station. For all white and grey boxes, equation (21) was used, and for the hatched boxes in Figure 9a, bifractal models, equations (24) or (25), have been used since they fitted better.

or

$$\tau(q) = \begin{cases} q\alpha_1 + q_\times(\alpha_2 - \alpha_1) - 1 & q \leq q_\times \\ q\alpha_2 - 1 & q > q_\times \end{cases}. \quad (23)$$

If this behavior is translated into the $h(q)$ picture using equation (12), we obtain that $h(q)$ exhibits a plateau from $q = -\infty$ up to a certain $q_\times$ and decays hyperbolically for $q > q_\times$,

$$h(q) = \begin{cases} \alpha_1 & q \leq q_\times \\ q_\times(\alpha_1 - \alpha_2)\dfrac{1}{q} + \alpha_2 & q > q_\times \end{cases}, \quad (24)$$

or vice versa,

$$h(q) = \begin{cases} q_\times(\alpha_2 - \alpha_1)\dfrac{1}{q} + \alpha_1 & q \leq q_\times \\ \alpha_2 & q > q_\times \end{cases}. \quad (25)$$

Both versions of this bifractal model require three parameters. The multifractal spectrum is degenerated to two single points, thus its width can be defined as $\Delta\alpha = \alpha_1 - \alpha_2$. One example of a bifractal fit is shown in Figure 6d.

[37] We have fitted the $h(q)$ spectra in the range $-10 \leq q \leq 10$ for all 99 precipitation records and all 42 runoff records by equations (21) and (24) (or equation (25)). For all runoff records, the modified multiplicative cascade model fits best. For the precipitation records, equation (21) fits best in just 54 cases; Figure 6c shows an example where the fit is not good. Either equation (24) or equation (25)

could be used to fit the results of 27 precipitation records. However, 18 of the precipitation records could be fit neither by the modified multiplicative cascade model nor by the bifractal approach.

[38] We have determined the multifractality strength $\Delta\alpha$ for the 81 precipitation records where either the modified multiplicative cascade model or the bifractal description could be used and for all 42 runoff records. The corresponding histograms are shown in Figure 9. We find that there is no systematic dependence of the $\Delta\alpha$ values on the geographic region or on the climate zone. Again, the rivers in southern Germany also show a broad distribution. However, $\Delta\alpha$ seems to show a slightly decreasing tendency with increasing basin area. The average multifractality strength is significantly smaller for the precipitation records ($\Delta\alpha = 0.29 \pm 0.14$) than for the runoff records ($\Delta\alpha = 0.49 \pm 0.16$). Note that for 18 precipitation records $\Delta\alpha$ could not be determined, since neither the modified multiplicative cascade model nor the simple bifractal approach fit.

[39] To show that the multifractality is due to correlations and not due to a broad probability distribution of the values ϕ_i we have also studied randomly shuffled data, finding no significant multifractality. For the precipitation records this means that there must be significant higher-order correlations, since standard second-order correlations are very weak or absent ($h(2) \approx 0.5$) and the multifractality is not caused by a broad, non-Gaussian distribution.

[40] Finally, we like to note that $h(q)$ for the precipitation records remains practically unchanged, when the seasonal detrending according to equation (2) instead of equation (1) is employed. This does not hold for rivers with strong

seasonal trends like those that nearly dry up in summer or freeze in winter. In this case, $h(q)$ is shifted toward higher values by a constant, which ranges between 0.1 and 0.25, but such that the strength $\Delta\alpha$ of the multifractality remains unchanged. We are not convinced, however, that equation (2) is the better way of removing seasonal periodicities in case of a multifractal analysis. In the multifractal description, $h(q)$ for negative q characterizes the scaling behavior of the small fluctuations, while $h(q)$ for positive q characterizes the scaling behavior of the large fluctuations. Thus the multifractal analysis can distinguish the scaling of small and large fluctuations. Now, if we divide by the seasonal trend in the standard deviation, following equation (2), some small fluctuations are rendered large and some large fluctuations are rendered small. Hence we believe that some of the information provided by a multifractal analysis is obscured this way.

6. Summary and Conclusion

[41] In summary, we have analyzed long precipitation records and long river discharge records using detrended fluctuation analysis (DFA) and its multifractal counterpart (MF-DFA). We find that the precipitation records are characterized by $h(2) \approx 1/2$, indicating a fast decay of the autocorrelation function, while the runoff records are long-term correlated above a crossover timescale of several weeks with fluctuation exponents $h(2)$ varying in a broad range. This result is rather surprising, since the fluctuations of rainfall are often claimed to play an important role in the long-term correlated (persistent) fluctuations of the runoff. Our study seems to indicate that the persistence of the runoff is not so much related with persistence in precipitation, but is rather caused by storage processes occurring in the soil and the highly intermittent spatial behavior of the rainfall. Further more extensive studies are needed to prove this conclusion.

[42] We also find that the runoff records are characterized, at large timescales, by a stronger average multifractality than the precipitation records. The multifractality strength is characterized by the difference $\Delta\alpha$ between the maximum and minimum Hölder exponent α needed for the characterization of the data. The type of multifractality occurring in all runoff records is consistent with a modified version of the binomial multifractal model, which supports the idea of a "universal" multifractal behavior of river runoffs suggested by S. Lovejoy and D. Schertzer in a different context. In contrast, 45% of the precipitation records seem to require a different description, and a simple bifractal fit can be used in 27% of all cases. For positive moments, the three-parameter Lovejoy-Schertzer approach always yields a good fit to the data. The multifractal exponents can be regarded as "fingerprints" for each station and can be used for testing the state-of-the-art precipitation-runoff models.

References

Andrade, R. F. S., H.-J. Schellnhuber, and M. Claussen (1998), Analysis of rainfall records: Possible relation to self-organized criticality, *Physica A*, *254*, 557–568.

Arneodo, A., B. Audit, N. Decoster, J.-F. Muzy, and C. Vaillant (2002), Wavelet based multifractal formalism: Applications to DNA sequences, satellite images of the cloud structure, and stock market data, in *The Science of Disaster: Climate Disruptions, Market Crashes, and Heart Attacks*, edited by A. Bunde, J. Kropp, and H.-J. Schellnhuber, pp. 27–102, Springer, New York.

Bhatthacharya, R. N., and E. C. Waymire (1990), *Stochastic Processes With Applications*, pp. 53–62, John Wiley, Hoboken, N. J.

Bhatthacharya, R. N., V. K. Gupta, and E. C. Waymire (1983), The Hurst effect under trends, *J. Appl. Probab.*, *20*, 649–662.

Bunde, A., S. Havlin, J. W. Kantelhardt, T. Penzel, J.-H. Peter, and K. Voigt (2000), Correlated and uncorrelated regions in heart-rate fluctuations during sleep, *Phys. Rev. Lett.*, *85*, 3736–3739.

Bunde, A., J. Kropp, and H.-J. Schellnhuber (Eds.) (2002), *The Science of Disaster: Climate Disruptions, Market Crashes, and Heart Attacks*, Springer, New York.

Chen, Z., P. C. Ivanov, K. Hu, and H. E. Stanley (2002), Effect of non-stationarities on detrended fluctuation analysis, *Phys. Rev. E*, *65*, 041107.

Davis, A., A. Marshak, W. Wiscombe, and R. Cahalan (1994), Multifractal characterization of nonstationarity and intermittency in geophysical fields: Observed, retrieved, or simulated, *J. Geophys. Res.*, *99*(D4), 8055–8072.

Davis, A., A. Marshak, W. Wiscombe, and R. Cahalan (1996), Multifractal characterization of intermittency in nonstationary geophysical signals and fields, in *Current Topics in Nonstationary Analysis*, edited by G. Trevino et al., pp. 97–158, World Sci., Hackensack, N. J.

Deidda, R. (2000), Rainfall downscaling in a space-time multifractal framework, *Water Resour. Res.*, *36*(7), 1779–1794.

Deidda, R., R. Benzi, and F. Siccardi (1999), Multifractal modeling of anomalous scaling laws in rainfall, *Water Resour. Res.*, *35*(6), 1853–1867.

Douglas, E. M., and A. P. Barros (2003), Probable maximum precipitation estimation using multifractals: Application in the eastern United States, *J. Hydrometeorol.*, *4*(6), 1012–1024.

Eichner, J. F., E. Koscielny-Bunde, A. Bunde, S. Havlin, and H.-J. Schellnhuber (2003), Power-law persistence and trends in the atmosphere: A detailed study of long temperature records, *Phys. Rev. E*, *68*, 046133.

Feder, J. (1988), *Fractals*, Springer, New York.

Feller, W. (1951), The asymptotic distribution of the range of sums of independent random variables, *Ann. Math. Stat.*, *22*, 427–432.

Fraedrich, K., and C. Larner (1993), Scaling regimes for composite rainfall time series, *Tellus, Ser. A*, *45*, 289–298.

Frisch, U., and G. Parisi (1985), Fully developed turbulence and intermittency, in *Turbulence and Predictability in Geophysical Fluid Dynamics*, edited by M. Ghil, R. Benzi, and G. Parisi, pp. 84–92, Elsevier, New York.

Gupta, V. K., and D. R. Dawdy (1995), Physical Interpretations of regional variations in the scaling exponents of flood quantiles, in *Scale Issues in Hydrological Modelling*, edited by J. D. Kalma, pp. 106–119, John Wiley, Hoboken, N. J.

Harris, D., M. Menabde, A. Seed, and G. Austin (1996), Multifractal characterization of rain fields with a strong orographic influence, *J. Geophys. Res.*, *101*(D21), 26,405–26,414.

Hu, K., P. Ch. Ivanov, Z. Chen, P. Carpena, and H. E. Stanley (2001), Effect of trends on detrended fluctuation analysis, *Phys. Rev. E*, *64*, 011114.

Hurst, H. E. (1951), Long-term storage capacity of reservoirs, *Trans. Am. Soc. Civ. Eng.*, *116*, 770–799.

Hurst, H. E., R. P. Black, and Y. M. Simaika (1965), *Long-Term Storage: An Experimental Study*, Constable, London.

Kantelhardt, J. W., E. Koscielny-Bunde, H. H. A. Rego, S. Havlin, and A. Bunde (2001), Detecting long-range correlations with detrended fluctuation analysis, *Physica A*, *295*, 441–454.

Kantelhardt, J. W., S. A. Zschiegner, E. Koscielny-Bunde, S. Havlin, A. Bunde, and H. E. Stanley (2002), Multifractal detrended fluctuation analysis of non-stationary time series, *Physica A*, *316*, 87–114.

Kantelhardt, J. W., D. Rybski, S. A. Zschiegner, P. Braun, E. Koscielny-Bunde, V. Livina, S. Havlin, and A. Bunde (2003), Multifractality of river runoff and precipitation: Comparison of fluctuation analysis and wavelet methods, *Physica A*, *330*, 240–245.

Klemes, V. (1974), The Hurst phenomenon: A puzzle?, *Water Resour. Res.*, *10*(4), 675–688.

Koscielny-Bunde, E., A. Bunde, S. Havlin, H. E. Roman, Y. Goldreich, and H.-J. Schellnhuber (1998), Indication of a universal persistence law governing atmospheric variability, *Phys. Rev. Lett.*, *81*, 729–732.

Koscielny-Bunde, E., J. W. Kantelhardt, P. Braun, A. Bunde, and S. Havlin (2006), Long-term persistence and multifractality of river runoff records:

Detrended fluctuation studies, *J. Hydrol.*, doi:10.1016/j.jhydrol.2005.03.004, in press.

Kumar, P., and E. Foufoula-Georgiou (1997), Wavelet analysis for geophysical applications, *Rev. Geophys.*, *35*(4), 385–412.

Künsch, H. R. (1986), Discrimination between monotonic trends and long-range dependence, *J. Appl. Probab.*, *23*, 1025–1030.

Lastovicka, J., P. Krizan, P. Sauli, and D. Novotna (2003), Persistence of the planetary wave type oscillations in foF_2 over Europe, *Ann. Geophys.*, *21*(7), 1543–1552.

Lavallee, D., S. Lovejoy, and D. Schertzer (1993), Nonlinear variability and landscape topography: Analysis and simulation, in *Fractals in Geography*, edited by L. DeCola and N. Lam, pp. 158–192, Prentice-Hall, Upper Saddle River, N. J.

Lovejoy, S., and B. Mandelbrot (1985), Fractal properties of rain and a fractal model, *Tellus, Ser. A*, *37*, 209–232.

Lovejoy, S., and D. Schertzer (1995), Multifractals and rain, in *New Uncertainty Concepts in Hydrology and Water Resources*, edited by Z. W. Kunzewicz, pp. 61–103, Cambridge Univ. Press, New York.

Mandelbrot, B. B., and J. R. Wallis (1968), Noah, Joseph, and operational hydrology, *Water Resour. Res.*, *4*(5), 909–918.

Mandelbrot, B. B., and J. R. Wallis (1969), Some long-run properties of geophysical records, *Water Resour. Res.*, *5*(2), 321–340.

Marani, M. (2003), On the correlation structure of continuous and discrete point rainfall, *Water Resour. Res.*, *39*(5), 1128, doi:10.1029/2002WR001456.

Matsoukas, C., S. Islam, and I. Rodriguez-Iturbe (2000), Detrended fluctuation analysis of rainfall and streamflow time series, *J. Geophys. Res.*, *105*(D23), 29,165–29,172.

Mesa, O. J., and G. Poveda (1993), The Hurst effect: The scale of fluctuation approach, *Water Resour. Res.*, *29*(12), 3995–4002.

Muzy, J. F., E. Bacry, and A. Arneodo (1991), Wavelets and multifractal formalism for singular signals: Application to turbulence data, *Phys. Rev. Lett.*, *67*, 3515–3518.

Olsson, J., V. P. Singh, and K. Jinno (1999), Effect of spatial averaging on temporal statistical and scaling properties of rainfall, *J. Geophys. Res.*, *104*(D16), 19,117–19,126.

Pandey, G., S. Lovejoy, and D. Schertzer (1998), Multifractal analysis of daily river flows including extremes for basins of five to two million square kilometers, one day to 75 years, *J. Hydrol.*, *208*, 62–81.

Peng, C.-K., S. V. Buldyrev, S. Havlin, M. Simons, H. E. Stanley, and A. L. Goldberger (1994), Mosaic organization of DNA nucleotides, *Phys. Rev. E*, *49*, 1685–1689.

Peters, O., and K. Christensen (2002), Rain: Relaxations in the sky, *Phys. Rev. E*, *66*, 036120.

Peters, O., C. Hertlein, and K. Christensen (2002), A complexity view of rainfall, *Phys. Rev. Lett.*, *88*, 018701.

Potter, K. W. (1976), Evidence for nonstationarity as a physical explanation of the Hurst phenomenon, *Water Resour. Res.*, *12*(5), 1047–1052.

Rangarajan, G., and M. Ding (2000), Integrated approach to the assessment of long range correlation in time series data, *Phys. Rev. E*, *61*, 4991–5001.

Rodriguez-Iturbe, I., and A. Rinaldo (1997), *Fractal River Basins: Change and Self-Organization*, Cambridge Univ. Press, New York.

Salas, J. D., D. C. Boes, V. Yevjevich, and G. G. S. Pegram (1979), Hurst phenomenon as a pre-asymptotic behavior, *J. Hydrol.*, *44*, 1–15.

Schertzer, D., and S. Lovejoy (1987), Physical modelling and analysis of rain and clouds by anisotropic scaling multiplicative processes, *J. Geophys. Res.*, *92*(D8), 9693–9714.

Schertzer, D., and S. Lovejoy (1991), *Nonlinear Variability in Geophysics: Scaling and Fractals*, Springer, New York.

Schertzer, D., S. Lovejoy, F. Schmitt, Y. Chigirinskaya, and D. Marsan (1997), Multifractal cascade dynamics and turbulent intermittency, *Fractals*, *5*(3), 427–471.

Schmitt, F., S. Vannitsem, and A. Barbosa (1998), Modeling of rainfall time series using two-state renewal processes and multifractals, *J. Geophys. Res.*, *103*(D18), 23,181–23,193.

Talkner, P., and R. O. Weber (2000), Power spectrum and detrended fluctuation analysis: Application to daily temperatures, *Phys. Rev. E*, *62*, 150–160.

Tchiguirinskaia, I., P. Hubert, H. Bendjoudi, and D. Schertzer (2002), Multifractal modeling of river runoff and seasonal periodicity, in *Preventing & Fighting Hydrological Disasters*, Orisonturi Univ., Timisoara, Romania.

Tessier, Y., S. Lovejoy, and D. Schertzer (1993), Universal multifractals: Theory and observations for rain and clouds, *J. Appl. Meteorol.*, *32*(2), 223–250.

Tessier, Y., S. Lovejoy, P. Hubert, D. Schertzer, and S. Pecknold (1996), Multifractal analysis and modelling of rainfall and river flows and scaling, causal transfer functions, *J. Geophys. Res.*, *101*(D21), 26,427–26,440.

Veneziano, D., and V. Iacobellis (2002), Multiscaling pulse representation of temporal rainfall, *Water Resour. Res.*, *38*(8), 1138, doi:10.1029/2001WR000522.

Veneziano, D., R. L. Bras, and J. D. Niemann (1996), Nonlinearity and self-similarity of rainfall in time and a stochastic model, *J. Geophys. Res.*, *101*(D21), 26,371–26,392.

Weber, R. O., and P. Talkner (2001), Spectra and correlations of climate data from days to decades, *J. Geophys. Res.*, *106*(D17), 20,131–20,144.

―――――――――――

P. Braun, Bayerisches Landesamt für Wasserwirtschaft, Lazarettstrasse 67, D-80636 München, Germany.

A. Bunde, E. Koscielny-Bunde, and D. Rybski, Institut für Theoretische Physik III, Justus-Liebig-Universität, Heinrich-Buff-Ring 16, D-35392 Giessen, Germany.

S. Havlin, Department of Physics and Minerva Center, Bar-Ilan University, Ramat-Gan 52900, Israel.

J. W. Kantelhardt, Fachgruppe Theorie, Fachbereich Physik, Universität Halle, D-06099 Halle (Saale), Germany. (kantelhardt@physik.uni-halle.de)